1 2	A structural model of the active ribosome-bound membrane protein
3	insertase YidC
4	
5	Stephan Wickles ¹ , Abhishek Singharoy ³ , Jessica Andreani ^{1,2} , Stefan Seemayer ¹ ,
6	Lukas Bischoff ¹ , Otto Berninghausen ¹ , Johannes Söding ^{1,2} , Klaus Schulten ³ , Eli
7	O. van der Sluis ^{1,*} and Roland Beckmann ^{1,*}
8	
9	¹ Gene Center Munich and Center for integrated Protein Science Munich, Department
10	of Biochemistry, Ludwig-Maximilians-Universität München, Feodor-Lynen-Straße
11	25, 81377 Munich, Germany
12	
13	² Max-Planck-Institute for Biophysical Chemistry, Am Faßberg 11, 37077 Göttingen,
14	Germany
15	
16	³ Beckman Institute for Advanced Science and Technology, University of Illinois
17	at Urbana-Champaign, 405 N. Mathews Ave, Urbana Illinois 61801, USA
18 19 20	* to whom correspondence should be addressed:
21 22	beckmann@lmb.uni-muenchen.de, vandersluis@lmb.uni-muenchen.de

23

24 SUMMARY

25

26 The integration of most membrane proteins into the cytoplasmic membrane of 27 bacteria occurs co-translationally. The universally conserved YidC protein 28 mediates this process either individually as a membrane protein insertase, or in 29 concert with the SecY complex (Dalbey et al. 2011; Kol et al. 2008). Here, we 30 present a structural model of YidC based on evolutionary co-variation analysis 31 (Hopf et al. 2012), lipid-versus-protein-exposure (Lai et al. 2013) and molecular 32 dynamics simulations. The model suggests a distinctive arrangement of the 33 conserved five transmembrane domains and a helical hairpin between 34 transmembrane segment 2 (TM2) and TM3 on the cytoplasmic membrane 35 surface. The model was used for docking into a cryo-electron microscopy 36 reconstruction of a translating YidC-ribosome complex carrying the YidC 37 substrate F_0c . This structure reveals how a single copy of YidC interacts with the 38 ribosome at the ribosomal tunnel exit and identifies a site for membrane protein 39 insertion at the YidC protein-lipid interface. Together, these data suggest a 40 mechanism for the co-translational mode of YidC-mediated membrane protein 41 insertion.

43

44 **TEXT**

45 At present, a mechanistic understanding of the function of YidC, as well as its 46 mitochondrial and chloroplast counterparts Oxa1 and Alb3, respectively, is 47 limited by a lack of structural information. High resolution structures are 48 available only for the first periplasmic domain (P1) of *Escherichia coli* YidC (Fig. 49 1a) (Oliver and Paetzel 2008; Ravaud et al. 2008), however, this domain is poorly 50 conserved, only present in Gram-negative bacteria and not essential for 51 functionality (Jiang et al. 2003). Furthermore, the region(s) of YidC mediating the 52 interaction with the ribosome have not been identified, and the oligomeric state 53 of YidC during co-translational translocation remains controversial (Herrmann 54 2013; Kedrov et al. 2013; Kohler et al. 2009). Hence, we set out to determine a 55 molecular model of ribosome-bound YidC during co-translational translocation 56 of the substrate F_{0c} (van der Laan et al. 2004), an integral membrane subunit of 57 the ATP synthase complex.

58 In order to build an initial structural model of YidC, we predicted contacts 59 between pairs of residues based on covariation analysis (Hopf et al. 2012; Marks 60 et al. 2011). For that purpose, we constructed a multiple sequence alignment of 61 E. coli YidC excluding the nonconserved first transmembrane helix (TM1) and 62 the P1 domain (Fig. 1a) and computed direct evolutionary couplings between 63 pairs of YidC residues (Kamisetty et al. 2013). The resulting matrix of coupling 64 strengths (Fig. 1b) contains several diagonal and anti-diagonal patterns of 65 stronger coupling coefficients, which are indicative of parallel or anti-parallel 66 helix-helix pairs, respectively. We computed probabilities for each possible helix-67 helix contact by aggregating the evidence of stronger coupling coefficients over 68 the expected interaction patterns and calibrating the resulting raw scores on an 69 independent dataset of helix-helix interactions to obtain accurate interaction 70 probabilities. Seven helix-helix contacts attained probabilities above 57% (Fig. 71 1b-d) while all other possible contacts scored below 15%, demonstrating the 72 specificity of the method (Fig. 1-figure supplement 1b).

We roughly positioned the five TM helices of *E. coli* YidC relative to each other using the predicted helix-helix contacts as constraints, and rotated them according to their predicted lipid or protein exposure (Lai et al. 2013) (Fig. 1c). 76 Next, we used MODELLER (Eswar et al. 2008) to create full length models based 77 on the TM core, secondary structure prediction and the 50 residue-residue 78 contacts with the highest coupling coefficients (39 excluding intrahelical 79 contacts, indels and topology violations). In the resulting model (Fig. 1e & f), the 80 conserved membrane integrated core of YidC forms a helical bundle arranged 81 like the vertices of a pentagon, in the order 4-5-3-2-6 (clockwise) when viewed 82 from the cytoplasm (Fig. 1f). Notably, all the predicted interactions between TM 83 domains can be explained by monomeric YidC suggesting that dimer or oligomer 84 formation may not be strictly required for YidC activity (see also below).

Outside the membrane region, strong helix-helix contacts were predicted within the cytoplasmic loop between TM2 and TM3, which can be explained the by formation of a helical hairpin (Fig. 1f). The base of this "helical paddle domain" (HPD) is structurally constrained by predicted contacts with TM3, its tip on the other hand is more mobile and appears to interact with lipid headgroups (see below).

91 While this manuscript was under review, two crystal structures were published 92 of *Bacillus halodurans* YidC2 (BhYidC2, 34% sequence identity with *E. coli* YidC) 93 (Kumazaki et al. 2014), providing us with a unique opportunity to directly assess 94 the accuracy of our model. Overall, the root mean square deviation (RMSD) between the TM helices of our model and those of BhYidC2 is 7.5 Å (3WO6) and 95 96 7.3 Å (3W07), which is within the resolution limits of our method. The global 97 arrangement of TM helices is the same as in BhYidC2, yet, their tilt angle relative 98 to the plane of the membrane is slightly different (Fig. 2). The tilt angle of the 99 HPD also differs, as well as its side that faces the membrane (Video 1), which 100 may be indicative of a high degree of flexibility of this domain, consistent with its 101 high crystallographic B-factors (Kumazaki et al. 2014). Notably, the HPD is not 102 essential for YidC function in *E. coli* since the deletion of the entire domain is 103 possible without compromising cell viability (Jiang et al. 2003).

A qualitative difference between our model and BhYidC2 that may have more mechanistic importance is the relative position of TM3. In the structure of BhYidC2 a hydrophilic groove is formed on the cytoplasmic side of the TM bundle that has been proposed to form a binding site for YidC substrates (Kumazaki et al. 2014). Interestingly, the opening state of this groove differs

109 between the two crystal forms, *i.e.* it is more open in 3W06 than in 3W07 (Video 110 1), largely due to movement of the N-terminal half of TM3 (Fig. 2-figure 111 supplement 1). In our model on the other hand, this hydrophilic groove is even 112 more closed than in 3W07 because we imposed covariation-based constraints 113 between TM3 and TM5 (Pro⁴²⁵-Pro⁴⁹⁹) and between TM3 and TM6 (Cys⁴²³-Gln⁵²⁸ 114 & Phe⁴³³-Thr⁵²⁴) (Fig. 2 and Video 1). Strikingly, in BhYidC2 the distances 115 between the $C\beta$ atoms of these three pairs are outliers compared to other 116 residue-residue pairs (20.5 Å/20.9 Å/14.9 Å vs an average of 8.2 Å, Fig. 2-figure supplement 2). Thus, given that (i) the position of TM3 differs in the two crystal 117 118 forms, and (ii) that covariation analysis predicts with high accuracy a closer 119 interaction of TM3 with TM6 and one contact with TM5, we conclude that 120 movement of TM3 is a genuine feature of YidC. This movement and the 121 accompanying dynamics of the hydrophilic groove may represent a crucial step 122 in the functional cycle of the YidC insertase.

123 In summary, the overall structure of our YidC model agrees well with the 124 BhYidC2 crystal structure, and a comparison of both structures reveals dynamic 125 regions in YidC that may be of mechanistic importance. This further illustrates 126 the power of covariation analysis not merely for structure prediction but also for 127 obtaining dynamic insights (Hopf et al. 2012).

128 Next, in order to further characterize and validate our obtained YidC model, we 129 assessed its stability and biochemical properties in the bacterial membrane by 130 employing traditional molecular dynamics (MD) simulations. Overall, the model 131 was found to be very stable during the simulation. While the five TM helices 132 enable a rigid protein core, the polar loop regions tend to swim on the 133 membrane surface (Fig. 3a). An analysis of inter-residue interactions within the 134 TM region (Fig. 3b) provides a firm basis to the observed stability of YidC: 135 hydrophobic residues on the exterior of the TM bundle stabilize interactions 136 with the apolar lipid tails. The YidC core, in turn, is stabilized both via short and 137 long-range interactions between the five helices. Residues towards the 138 cytoplasmic side of the core are primarily polar or charged and, therefore, 139 engaged in strong electrostatic or charge-dipole interactions. In contrast, 140 residues on the periplasmic side are primarily aromatic and involved in stacking 141 and other nonpolar dispersion interactions.

142 In order to verify the functional relevance of residues suggested by the MD 143 simulations, we created alanine mutants and subjected them to an *in vivo* 144 complementation assay. Some of the most stabilizing residues, T362 in TM2 and 145 Y517 in TM6, both of which are located at the same height in the membrane, 146 completely inactivated YidC when mutated to alanine (Fig. 3d & Fig. 3-figure 147 supplement 1). Both mutants were stably expressed, indicating that the lack of 148 complementation was not caused by instability of YidC (Fig. 3-figure supplement 149 2). Several residues close to this pair show intermediate activity levels (F433, 150 M471 and F505), whereas residues further away do not show an effect (Fig. 3-151 figure supplement 1). Taken together, we provide a model for the overall 152 arrangement of the conserved domains of YidC that is in good agreement with 153 our covariation analysis, lipid exposure prediction, MD simulation, in vivo 154 complementation analysis as well as the recent crystal structures.

155 Interestingly, we observed that YidC induces thinning of the lipid bilayer during the MD simulation. A significant thinning of 7-10 Å results from the hydrophobic 156 157 mismatch between the TM helices and the membrane (Fig. 3e). The thinning is 158 similar in the upper and lower leaflet, and the thinnest region is in proximity of 159 TM3 and TM5. Since membrane inserting YidC substrates have been chemically 160 cross-linked to both these helices (Klenner and Kuhn 2012; Klenner et al. 2008; 161 Yu et al. 2008), we argue that thinning of this region in particular may be 162 relevant for the molecular mechanism of YidC-dependent membrane insertion. 163 In addition, the distribution of hydrophilic and hydrophobic residues within YidC 164 revealed the presence of a hydrophilic environment on the cytoplasmic side of 165 the YidC TM bundle (Fig. 3f), which continues into the mentioned hydrophobic 166 cluster of aromatic residues towards the periplasmic side. It is tempting to 167 speculate that this hydrophilic environment may receive the polar termini and 168 loops of YidC substrates during the initiation of translocation, thus facilitating 169 their transfer across the hydrophobic core of the (thinned) lipid bilayer (see 170 below). Notably, essentially the same conclusions have been drawn on the basis 171 of the BhYidC2 crystal structures and accompanying cross-linking studies 172 (Kumazaki et al. 2014).

In order to provide a molecular model of YidC in its active state, we reconstituted
purified full length YidC (extended with the C-terminus of *R. baltica* YidC (Seitl et

175 al. 2014)) with ribosome nascent chains (RNCs) exposing the first TM helix of 176 $F_{0}c$, and subjected the complex to cryo-EM and single particle analysis to a resolution of ~8 Å (Fig. 4a & b). In agreement with previous structural studies 177 178 (Kohler et al. 2009; Seitl et al. 2014), YidC binds to the ribosomal exit site, 179 however, the improved resolution now allows for a more detailed interpretation. 180 Firstly, we were able to separate the weaker electron density of the detergent 181 micelle from that of YidC (Fig. 4a). Secondly, the presence of elongated structural 182 features (Fig. 4d-f) allowed us to dock our molecular model in a distinct 183 orientation (cross correlation coefficient 0.865). Following placement of the 184 YidC-core model, two prominent densities in the membrane region, one next to 185 TM3 and one next to TM5, remained unaccounted for. These could be attributed 186 to either TM1 of YidC or to the TM helix of the nascent chain (NC) F_0c . Given that 187 (i) YidC substrates are known to crosslink to TM3 (Klenner and Kuhn 2012; 188 Klenner et al. 2008; Yu et al. 2008), and (ii) that the density neighboring TM3 is 189 aligned with the ribosomal exit tunnel and (iii) that at the same relative position 190 nascent chains have been observed inside the SecY channel (Frauenfeld et al. 191 2011) (Fig. 4-figure supplement 1), the most plausible assignment to the density 192 near TM3 appeared to be the TM helix of F_0c . To verify this, and to exclude that 193 the density neighboring TM5 corresponds to the nascent chain, we reconstituted 194 single cysteine mutants of YidC either in TM3 (M430C and P431C) or in TM5 195 (V500C and T503C) with RNCs of a single cysteine mutant of $F_0c(G23C)$, and 196 exposed them to disulphide crosslinking. Upon exposure to the oxidator DTNB, 197 only in the TM3 mutants a DTT-sensitive ~90 kDa product appeared that reacted 198 with antibodies against the nascent chain (NC-tRNA~30 kDa, Fig. 4c) as well as 199 YidC (~60 kDa, Fig. 4c). Thus, the adduct represented indeed the inserting F_{0C} 200 TM domain crosslinked to TM3 of YidC. RNCs lacking a cysteine in the nascent 201 chain (Fig. 4-figure supplement 2) or YidC mutants with cysteines in TM5 did not 202 yield any crosslinks (Fig. 4c). Hence, we conclude that the unaccounted electron 203 density next to TM3 represents the TM of the nascent chain, and that the density 204 neighbouring TM5 represents TM1 of YidC (Fig. 4d-f).

We attribute the remaining unaccounted electron density in the periplasmic region to the P1 domain; however, because it is substantially smaller than the crystal structure of P1, we did not include it in our molecular model. Flexibility relative to the conserved membrane region of YidC is the most likely explanation
for this finding. We did not observe density for the HPD, in agreement with its
flexibility observed in both, the crystal structures of BhYidC2 and the MD
simulations (Fig. 3c).

212 In order to validate our molecular model of co-translationally active YidC, we 213 mutated residues that would be in direct contact with the ribosome (Fig. 5a & b) 214 and analyzed their effect on functionality in the *in vivo* complementation test. 215 Indeed, mutation of residues Y370A and Y377A (contacting ribosomal RNA helix 216 59) and D488K (contacting ribosomal protein uL23) severely interfere with YidC 217 activity (Fig. 5c & Fig. 5-figure supplement 1) thereby emphasizing their 218 functional significance. All these mutants were stably expressed, indicating that 219 the lack of complementation was not caused by instability of YidC (Fig. 5-figure 220 supplement 2). Given that YidC in general is known to be very tolerant to point 221 mutations (Jiang et al. 2003), this provides further support for the overall 222 correctness of our model of ribosome-bound YidC during membrane protein 223 insertion.

224 Finally, it is notable that we observe only a single monomer of YidC bound to the 225 active ribosome. This is in agreement with recent literature showing clearly that 226 both YidC (Herrmann 2013; Kedrov et al. 2013; Seitl et al. 2014) and the SecY 227 complex (Frauenfeld et al. 2011; Park et al. 2014; Park and Rapoport 2012; 228 Taufik et al. 2013) can be fully active as monomers. However, the comparison of 229 models for active YidC and active SecY (Fig. 5e & Fig. 4-figure supplement 1) 230 reveals an important difference between the two proteins that has mechanistic 231 implications. While SecY is known to translocate hydrophilic nascent chains 232 through its central aqueous channel (Cannon et al. 2005; Driessen and Nouwen 233 2008; Rapoport 2007) and insert TM domains through a lateral gate (Gogala et 234 al. 2014; Van den Berg et al. 2004), our model suggests that the YidC substrates 235 are inserted at the protein-lipid interface. Two principal findings of our work 236 suggest how YidC may facilitate this process: (i) it provides a hydrophilic 237 environment within the membrane core for receiving the hydrophilic moieties 238 (termini or loops) of a substrate, and (ii) it reduces the thickness of the lipid 239 bilayer: initial interaction of the hydrophilic moieties of YidC substrates with the 240 hydrophilic environment of YidC would allow for a partial insertion into the

241 membrane, while facilitating exposure of the hydrophobic TM domains to the 242 hydrophobic core of the bilayer. The latter in turn may compensate for the 243 energetic penalty of driving the hydrophilic moieties across the (already 244 thinned) bilayer. Further biochemical and structural studies that capture the 245 earlier stages of this translocation process are eagerly awaited to fully elucidate 246 this mechanism.

249 METHODS

250

251 Covariation analysis

252 We constructed a multiple sequence alignment of YidC excluding the unconserved 253 first transmembrane helix (TM1) and the periplasmic P1 domain. We searched for 254 homologous sequences of E. coli YidC starting from the PFAM seed alignment of 255 family PF02096 (Punta et al. 2012) and using the sensitive homology detection 256 software HHblits (Remmert et al. 2012). First, 5 iterations of HHblits were run 257 against the clustered Uniprot database with no filtering, to retrieve as many 258 homologous sequences as possible. Then, we post-processed the alignment using 259 HHfilter to generate a non-redundant alignment at 90% sequence identity. This 260 resulted in an alignment containing 2366 sequences aligned across YidC helices 261 TM2-TM6. Using this multiple sequence alignment, we computed direct evolutionary 262 couplings between pairs of YidC residues using the method of Kamisetty et al 263 (Kamisetty et al. 2013).

264 To compute probabilities for each possible helix-helix contact, we aggregated the 265 evidence of stronger coupling coefficients over the expected interaction patterns for 266 helix-helix contacts, taking into account the expected periodicity of ~3.5 residues per 267 alpha helix turn. We built three non-redundant datasets of mainly-alpha proteins from 268 the CATH database (Sillitoe et al. 2013). For each protein, we slid a square pattern (of 269 size 17x17 residues = 289 cells) over the matrix of coupling strengths. For each 270 pattern position, we used Bayes theorem to calculate the raw probability for a helix-271 helix interaction, given the 289 coupling strengths. The distributions of coupling 272 strengths for interacting and non-interacting helix residues were fitted on dataset #1 273 (1118 proteins). We assigned different weights to the pattern cells, depending on their 274 position within the pattern and the direction of the helix-helix interaction (parallel or 275 antiparallel); these weights were optimized on dataset #2 (204 proteins). Finally, we 276 calibrated the resulting raw scores on dataset #3 (85 proteins) to obtain accurate 277 interaction probabilities. For cross-validation purposes, we also performed 278 optimization on dataset #3 and calibration on dataset #2. Optimization on either 279 dataset #2 or dataset #3 results in the same choice of weights for the pattern cells. The 280 final posterior probabilities were obtained as the average of the values calibrated on 281 datasets #2 and #3, weighted by dataset size. The calibration plots for datasets #2 and

#3 are shown in Fig. 1-figure supplement 1a. The histogram of final posterior
probabilities obtained for YidC is shown in Fig. 1-figure supplement 1b, which
illustrates the specificity of the helix-helix predictions.

285

286 YidC initial model building

287 The conserved TM helices of *E.coli* YidC were positioned according to the 288 covariation based helix-helix contact prediction, and rotated based on their predicted 289 lipid or protein exposure (Lai et al. 2013), resulting in a starting model of the 290 conserved TM core of YidC. Additional information based on direct residue-residue 291 interactions (covariance analysis) and secondary structure predictions by Jpred 3 292 (Cole et al. 2008) were used as structural restraints in MODELLER (Eswar et al. 293 2008). From a total of 10 output models that differed mainly in the relative orientation 294 of the loop regions, the model that satisfied the imposed constraints best was used for 295 further studies.

296

297 Molecular dynamics simulation

298 System preparation

299 All simulations were performed with the MD software NAMD 2.9 using the 300 CHARMM36 force field for the proteins and lipids (Klauda et al. 2010). The TIP3P 301 model is used to simulate water (Jorgensen et al. 1983). The YidC model was inserted 302 into the membrane, solvated, and ionized using the Membrane Builder tools on 303 CHARMM-GUI (Jo et al. 2008). The lipid composition is chosen to be 3 POPE to 1 304 POPG, as has been successfully used for modelling bacterial membranes in several 305 past MD simulations (Ash et al. 2004; Mondal et al. 2013). An initial membrane 306 surface of area 110 Å x 110 Å was constructed along the XY plane. The protein lipid-307 construct was solvated with 25 Å thick layers of water along the Cartesian Z 308 directions, and ionized to charge neutralization using Monte Carlo sampling of Na⁺ 309 and Cl⁻ ions at 0.15 M concentration. The overall system size is 0.15 M. Prior to 310 simulation the system was subjected to 10000 steps of conjugate gradient energy 311 minimization, followed by 100 ps of thermalization and 25 ns of equilibration. During 312 the first 10 ns of the equilibration stage, the protein was kept fixed, allowing the 313 lipids, ions and water molecules to equilibrate. Subsequent 15 ns of equilibration 314 included the protein as well. We then performed 500 ns of MD simulation at 300K.

The final 100 ns was repeated thrice to examine the statistical significance of the result.

317 *Simulation parameters*

318 The systems were kept at constant temperature using Langevin dynamics for all nonhydrogen atoms with a Langevin damping coefficient of 5ps⁻¹. A constant pressure of 319 320 latm was maintained using the Nose-Hoover Langevin piston with a period of 100fs 321 and damping timescale of 50fs. Simulations were performed with an integration time 322 step of 1fs where bonded interactions were computed every time step, short-range 323 non-bonded interactions every two time steps, and long range electrostatic 324 interactions every four time steps. A cutoff of 12 Å was used for van der Waals and 325 short-range electrostatic interactions: a switching function was started at 10 Å for van 326 der Waals interactions to ensure a smooth cutoff. The simulations were performed 327 under periodic boundary conditions, with full-system, long-range electrostatics 328 calculated by using the PME method with a grid point density of 1/Å. The unit cell 329 was large enough so that adjacent copies of the system did not interact via short-range 330 interactions.

331 Flexibility analysis

332 The overall flexibility of the transmembrane helices relative to their average 333 configuration was compared. Positional variance of the helix residues was quantified 334 as a measure of their flexibility. Positional variance was computed by summing the 335 deviation of individual backbone atom position and dividing by the number of 336 backbone atoms in the loop. This measure is slightly different from the usual root 337 mean square fluctuation (RMSF) as contributions from overall displacements of the 338 helices and their motions relative to the rotation/translation and internal motions of 339 the protein are included to probe flexibility.

340 Interaction energy, hydrogen bonds, and membrane thickness analysis

341 To further understand the details of the structure and dynamics of the YidC model we 342 performed interaction energy, hydrogen bond, and membrane thinning analysis. These 343 analyses were carried out on the MD trajectory using standard tools available on 344 VMD. In particular, interaction energies were computed for each trajectory frame of 345 the final 100 ns simulation using the NAMD Energy plugin on VMD. The numbers 346 were then time averaged over the entire 100ns, locally averaged for every residue 347 over a cut-off distance of 10 Å, and plotted on the structure in Fig. 3b. Hydrogen 348 bonds are defined solely on the basis of geometric parameters (bond angle: 20°; bondlength: 3.8 Å) between donors and acceptors. Thickness at a given point on the
membrane surface was probed by finding the nearest lipid head group and measuring
the minimum distance between the phosphate on that lipid head and one on the
opposite leaflet.

353

354 **Purification of ribosome nascent chain complexes (RNCs)**

355 RNC constructs encoding residues 1-46 of F_{OC} (preceded by an N-terminal His-tag 356 and 3C rhinoprotease cleavage site, and followed by an HA-tag and TnaC stalling 357 sequence) were cloned into a pBAD vector (Invitrogen) by standard molecular 358 biology techniques, and expressed and purified as described in Bischoff et al., 359 (submitted). Briefly, *E.coli* KC6 $\Delta smpB\Delta ssrA$ (Seidelt et al. 2009) carrying the 360 plasmid for F_oc was grown in LB with 100 μ g/ml ampicilin at 37°C to an OD₆₀₀ = 0.5 361 and expression was induced for 1h by adding 0.2 % arabinose. Cells were lysed and 362 debris was removed by centrifugation for 20 min at 16.000 rpm in a SS34-rotor 363 (Sorvall). The cleared lysate was spun overnight through a sucrose cushion at 45.000 364 rpm in a Ti45 rotor (Beckmann), the ribosomal pellet was resuspended for 1 h at 4°C 365 and RNCs were purified in batch by affinity purification using Talon (Clontech). 366 After washing the Talon beads with high salt buffer the RNCs were eluted and loaded 367 onto a linear 10 % - 40 % sucrose gradient. The 70S peak was collected, RNCs were 368 concentrated by pelleting, resuspended in an appropriate volume of RNC Buffer (20 369 mM HEPES pH 7.2, 100 mM KOAc, 6 mM MgOAc₂, 0.05% (w/v) dodecyl 370 maltoside), flash frozen in liquid N₂ and stored at -80°C. The complete sequence of 371 the nascent chain is:

372 MGHHHHHHHDYDIPTTLEVLFQGPGTMENLNMDLLYMAAAVMMGLAAI

373 GAAIGIGILGGKFLEGAARQPDLIYPYDVPDYAGPNILHISVTSKWFNIDNKIV374 DHRP

375

376 **Purification of YidC**

For purification and reconstitution studies, *E.coli* YidC extended with the C-terminus from *R. baltica* (Seitl et al. 2014) was re-cloned into pET-16 (Novagen) with an Nterminal His-tag followed by a 3C rhinovirus protease site. Expression and purification was performed essentially as described (Lotz et al. 2008). Briefly, *E.coli* C43(DE3) cells (Miroux and Walker 1996) harboring the YidC construct were grown at 37°C to an $OD_{600} = 0.6$ and expression was induced by adding 0.5 mM IPTG. YidC was solubilized with Cymal-6 (Anatrace) and purified by affinity chromatography
using TALON (Clontech). The N-terminal His-tag of the eluted protein was cleaved
off with 3C protease during overnight dialysis at 4°C, followed by gel filtration
chromatography (Superdex 200, GE Healthcare). Fractions of the monodisperse peak
were pooled, concentrated to ~ 1 mg/ml in YidC Buffer (20 mM NaPO₄ pH 6.8, 100
mM KOAc, 10 % glycerol, 0.05 % Cymal-6) and directly used for further structural
or biochemical assays.

390

391 Disulphide crosslinking

For disulphide crosslink analysis, $F_{0}c^{(G23C)}$ -RNCs and single cysteine mutants of 392 393 YidC were purified separately and reconstituted by incubating 100 pmol of RNCs 394 with 500 pmol of freshly purified YidC for 30 min at 37°C. The endogenous cysteine 395 in YidC at position 423 was replaced by serine. Disulphide crosslinking was induced 396 by adding 1 mM 5,5'-dithiobis-(2-nitrobenzoicacid) (DTNB) for 10 min at 4°C and 397 quenched by adding 20 mM N-Ethylmaleimide (NEM) for 20 min at 4°C. 398 Crosslinked RNC-YidC complexes were separated from non-crosslinked YidC using 399 a 10 % - 40 % linear sucrose gradient, and the 70S peak was harvested and analysed 400 by SDS-PAGE followed by western blotting.

401

402 Complementation assay

403 For in vivo complementation studies, wildtype E. coli YidC was recloned into 404 pTrc99a (Pharmacia), and mutants were created by standard molecular cloning 405 techniques. *E.coli* FTL10 cells (Hatzixanthis et al. 2003) harboring pTrc99a plasmids 406 encoding the YidC variants were grown overnight at 37°C in LB medium 407 supplemented with 100 μ g/ml ampiciline, 50 μ g/ml kanamycin and 0.2% arabinose. 408 YidC depletion was carried out by transferring the cells to LB medium supplemented 409 with 100 μ g/ml ampiciline, 50 μ g/ml kanamycin and 0.2% glucose, followed by and 410 additional incubation for 3h at 37°C. Cell suspensions of all constructs were adjusted 411 to $OD_{600} = 0.1$ and either loaded onto SDS-PAGE gels for subsequent Western blotting, or further diluted to $OD_{600} = 10^{-5}$. Each dilution was spotted on LB agar 412 413 plates supplemented 100 μ g/ml ampiciline, 50 μ g/ml kanamycin and either 0.2% 414 arabinose or 0.2% glucose, and incubated overnight at 37°C.

415

416 Electron microscopy and image processing

For cryo-EM analysis, F_0c -RNC:YidC complexes were reconstituted by incubating 10 pmol of RNCs with 100 pmol of freshly purified YidC for 30 min at 37°C in a final volume of 50 µl of RNC buffer. Samples were applied to carbon-coated holey grids according to standard methods (Wagenknecht et al. 1988). Micrographs were collected under low-dose conditions on a FEI TITAN KRIOS operating at 200 kV using a 4k x 4k TemCam-F416 CMOS camera and a final pixel size of 1.035Å on the object scale.

424 Image processing was done using the SPIDER software package (Shaikh et al. 2008). 425 The defocus was determined using the TF ED command in SPIDER followed by 426 automated particle picking using Signature (Chen and Grigorieff 2007). The machine-427 learning algorithm MAPPOS (Norousi et al. 2013) was used to subtract "false 428 positive" particles from the data set and initial alignment was performed using an 429 empty 70S ribosome as reference. The complete data set (876376 particles) was 430 sorted using competitive projection matching in SPIDER followed by focused sorting 431 for ligand density (Leidig et al. 2013), and refined to a final resolution of ~ 8.0 Å 432 (Fourier shell correlation (FSC) cut-off 0.5). The final dataset consisted of 58960 433 particles showing electron density for P-site tRNA and ligand density at the tunnel 434 exit.

435

437 Acknowledgements

We would like to thank C. Ungewickell for assistance with cryo-electron
microscopy, Susan Vorberg for assistance with covariation analyses, T. Palmer
for providing *E. coli* strain FTL10, A. Driessen and A. Kuhn for providing YidC
antibodies, J. Philippou-Massier and U. Gaul for use of the robotic high-throuput
facility, A. Heuer for assistance with animations and B. Beckert & A. Kedrov for
discussions.

- 444 SW and LB were supported by the International Max Planck Research School, SS 445 by grant GRK1721 from the DFG, JA by a Humboldt Research Felloship of the 446 Alexander-von-Humboldt Foundation and the Bavarian Network for Molecular 447 Biosystems (BioSysNet), AS by a Beckman Postdoctoral Fellowship, KS by the 448 Center for Macromolecular Modeling and Bioinformatics (NIH 9P41GM104601, 449 NIH R01-GM67887) and the Center for the Physics of Living Cells (NSF PHY-450 0822613), JS by the Deutsche Forschungsgemeinschaft (DFG) trough grants 451 SFB646, GRK1721, and QBM, by the Bundesministerium für Bildung und 452 Forschung through grant CoreSys and the Bavarian Network for Molecular 453 Biosystems (BioSysNet), and RB by the Center for Integrated Protein Science and 454 the European Research Council (Advanced Grant CRYOTRANSLATION).
- 455

456 Author contributions

457 SW performed purifications, reconstitutions, cryo-EM image processing and 458 model building, LB contributed to purifications and image processing, JA, SS and 459 JS performed covariation analyses, AS and KS performed MD simulations and 460 related analyses, OB performed cryo-EM data collection, EvdS designed 461 experiments and supervised the project together with RB. All authors 462 contributed to data interpretation and writing of the manuscript.

463

464 **REFERENCES**

- 465
- 466
- Ash, W. L., Zlomislic, M. R., Oloo, E. O. & Tieleman, D. P. 2004. Computer
 simulations of membrane proteins. *Biochim Biophys Acta* 1666, 158-189,
 doi:10.1016/j.bbamem.2004.04.012.
- 470 2 Cannon, K. S., Or, E., Clemons, W. M., Jr., Shibata, Y. & Rapoport, T. A. 2005.
 471 Disulfide bridge formation between SecY and a translocating polypeptide
 472 localizes the translocation pore to the center of SecY. *J Cell Biol* 169, 219473 225, doi:10.1083/jcb.200412019.
- 474 3 Chen, J. Z. & Grigorieff, N. 2007. SIGNATURE: a single-particle selection
 475 system for molecular electron microscopy. *J Struct Biol* 157, 168-173,
 476 doi:10.1016/j.jsb.2006.06.001.
- 477 4 Cole, C., Barber, J. D. & Barton, G. J. 2008. The Jpred 3 secondary structure
 478 prediction server. *Nucleic Acids Res* 36, W197-201,
 479 doi:10.1093/nar/gkn238.
- 4805Dalbey, R. E., Wang, P. & Kuhn, A. 2011. Assembly of bacterial inner481membrane proteins. Annu Rev BiochemBiochem482doi:10.1146/annurev-biochem-060409-092524.
- 483 6 Driessen, A. J. & Nouwen, N. 2008. Protein translocation across the
 484 bacterial cytoplasmic membrane. *Annu Rev Biochem* 77, 643-667,
 485 doi:10.1146/annurev.biochem.77.061606.160747.
- 486 7 Eswar, N., Eramian, D., Webb, B., Shen, M. Y. & Sali, A. 2008. Protein
 487 structure modeling with MODELLER. *Methods Mol Biol* 426, 145-159,
 488 doi:10.1007/978-1-60327-058-8_8.
- Frauenfeld, J. *et al.* 2011. Cryo-EM structure of the ribosome-SecYE complex in the membrane environment. *Nat Struct Mol Biol* 18, 614-621, doi:10.1038/nsmb.2026.
- 492 9 Gogala, M. *et al.* 2014. Structures of the Sec61 complex engaged in nascent
 493 peptide translocation or membrane insertion. *Nature* 506, 107-110,
 494 doi:10.1038/nature12950.
- Hatzixanthis, K., Palmer, T. & Sargent, F. 2003. A subset of bacterial inner
 membrane proteins integrated by the twin-arginine translocase. *Mol Microbiol* 49, 1377-1390.
- Herrmann, J. M. 2013. The bacterial membrane insertase YidC is a
 functional monomer and binds ribosomes in a nascent chain-dependent
 manner. *J Mol Biol* 425, 4071-4073, doi:10.1016/j.jmb.2013.08.003.
- 50112Hopf, T. A. et al. 2012. Three-dimensional structures of membrane502proteins from genomic sequencing. Cell 149, 1607-1621,503doi:10.1016/j.cell.2012.04.012.
- 50413Jiang, F. et al. 2003. Defining the regions of Escherichia coli YidC that505contribute to activity. J Biol Chem 278, 48965-48972,506doi:10.1074/jbc.M307362200.
- 507
 14
 Jo, S., Kim, T., Iyer, V. G. & Im, W. 2008. CHARMM-GUI: a web-based

 508
 graphical user interface for CHARMM. J Comput Chem 29, 1859-1865,

 509
 doi:10.1002/jcc.20945.
- 510 15 Jorgensen, W. L., Chandrasekhar, J., Madura, J. D., Impey, R. W. & Klein, M.
- 511 L. 1983. Comparison of Simple Potential Functions for Simulating Liquid

512 Water. Journal of Chemical **Physics** 79, 926-935, doi:Doi 513 10.1063/1.445869. 514 16 Kamisetty, H., Ovchinnikov, S. & Baker, D. 2013. Assessing the utility of 515 coevolution-based residue-residue contact predictions in a sequence- and 516 structure-rich era. Proc Natl Acad Sci U S A 110, 15674-15679, 517 doi:10.1073/pnas.1314045110. 518 17 Kedrov, A. et al. 2013. Elucidating the native architecture of the YidC: 519 ribosome complex. Mol Biol 425, 4112-4124, Ι 520 doi:10.1016/j.jmb.2013.07.042. Klauda, J. B. et al. 2010. Update of the CHARMM all-atom additive force 521 18 522 field for lipids: validation on six lipid types. J Phys Chem B 114, 7830-523 7843, doi:10.1021/jp101759q. 524 19 Klenner, C. & Kuhn, A. 2012. Dynamic disulfide scanning of the 525 membrane-inserting Pf3 coat protein reveals multiple YidC substrate 526 contacts. J Biol Chem 287, 3769-3776, doi:10.1074/jbc.M111.307223. 527 20 Klenner, C., Yuan, J., Dalbey, R. E. & Kuhn, A. 2008. The Pf3 coat protein 528 contacts TM1 and TM3 of YidC during membrane biogenesis. FEBS Lett 529 **582**, 3967-3972, doi:10.1016/j.febslet.2008.10.044. 530 21 Kohler, R. et al. 2009. YidC and Oxa1 form dimeric insertion pores on the 531 translating ribosome. Mol Cell 34. 344-353. 532 doi:10.1016/j.molcel.2009.04.019. 533 22 Kol, S., Nouwen, N. & Driessen, A. J. 2008. Mechanisms of YidC-mediated 534 insertion and assembly of multimeric membrane protein complexes. J Biol 535 *Chem* **283**, 31269-31273, doi:10.1074/jbc.R800029200. 536 23 Kumazaki, K. et al. 2014. Structural basis of Sec-independent membrane 537 protein insertion by YidC. *Nature*, doi:10.1038/nature13167. 538 24 Lai, J. S., Cheng, C. W., Lo, A., Sung, T. Y. & Hsu, W. L. 2013. Lipid exposure 539 prediction enhances the inference of rotational angles of transmembrane 540 helices. BMC Bioinformatics 14, 304, doi:10.1186/1471-2105-14-304. 541 25 Leidig, C. et al. 2013. Structural characterization of a eukaryotic 542 chaperone--the ribosome-associated complex. *Nat Struct Mol Biol* **20**, 23-543 28, doi:10.1038/nsmb.2447. 544 26 Lotz, M., Haase, W., Kuhlbrandt, W. & Collinson, I. 2008. Projection 545 structure of yidC: a conserved mediator of membrane protein assembly. *I* 546 *Mol Biol* **375**, 901-907, doi:10.1016/j.jmb.2007.10.089. 547 Marks, D. S. et al. 2011. Protein 3D structure computed from evolutionary 27 548 seauence variation. PLoS One e28766. 6. 549 doi:10.1371/journal.pone.0028766. 550 28 Miroux, B. & Walker, J. E. 1996. Over-production of proteins in Escherichia 551 coli: mutant hosts that allow synthesis of some membrane proteins and 552 globular proteins at high levels. *J Mol Biol* **260**, 289-298, 553 doi:10.1006/jmbi.1996.0399. 554 29 Mondal, S., Khelashvili, G., Shi, L. & Weinstein, H. 2013. The cost of living 555 in the membrane: a case study of hydrophobic mismatch for the multi-556 segment protein LeuT. Chem Phys 169, Lipids 27-38. 557 doi:10.1016/j.chemphyslip.2013.01.006. 558 30 Norousi, R. et al. 2013. Automatic post-picking using MAPPOS improves 559 particle image detection from cryo-EM micrographs. *J Struct Biol* **182**, 59-560 66, doi:10.1016/j.jsb.2013.02.008.

561 31 Oliver, D. C. & Paetzel, M. 2008. Crystal structure of the major periplasmic 562 domain of the bacterial membrane protein assembly facilitator YidC. J Biol 563 Chem 283, 5208-5216, doi:10.1074/jbc.M708936200. 564 32 Park, E. et al. 2014. Structure of the SecY channel during initiation of 565 protein translocation. *Nature* **506**, 102-106, doi:10.1038/nature12720. 566 Park, E. & Rapoport, T. A. 2012. Bacterial protein translocation requires 33 567 only one copy of the SecY complex in vivo. J Cell Biol 198, 881-893, 568 doi:10.1083/jcb.201205140. 569 34 Punta, M. et al. 2012. The Pfam protein families database. Nucleic Acids 570 *Res* **40**, D290-301, doi:10.1093/nar/gkr1065. 571 35 Rapoport, T. A. 2007. Protein translocation across the eukaryotic 572 endoplasmic reticulum and bacterial plasma membranes. Nature 450, 573 663-669, doi:10.1038/nature06384. 574 36 Ravaud, S., Stjepanovic, G., Wild, K. & Sinning, I. 2008. The crystal 575 structure of the periplasmic domain of the Escherichia coli membrane 576 protein insertase YidC contains a substrate binding cleft. [Biol Chem 283, 577 9350-9358, doi:10.1074/jbc.M710493200. 578 37 Remmert, M., Biegert, A., Hauser, A. & Soding, J. 2012. HHblits: lightning-579 fast iterative protein sequence searching by HMM-HMM alignment. Nat 580 *Methods* **9**, 173-175, doi:10.1038/nmeth.1818. 581 38 Seidelt, B. et al. 2009. Structural insight into nascent polypeptide chain-582 mediated translational stalling. Science 326, 1412-1415, 583 doi:10.1126/science.1177662. 584 39 Seitl, I., Wickles, S., Beckmann, R., Kuhn, A. & Kiefer, D. 2014. The C-585 terminal regions of YidC from Rhodopirellula baltica and Oceanicaulis 586 alexandrii bind to ribosomes and partially substitute for SRP receptor 587 function Escherichia coli. Mol Microbiol 91, in 408-421, 588 doi:10.1111/mmi.12465. 589 40 Shaikh, T. R. et al. 2008. SPIDER image processing for single-particle 590 reconstruction of biological macromolecules from electron micrographs. 591 *Nat Protoc* **3**, 1941-1974, doi:10.1038/nprot.2008.156. 592 41 Sillitoe, I. et al. 2013. New functional families (FunFams) in CATH to 593 improve the mapping of conserved functional sites to 3D structures. 594 *Nucleic Acids Res* **41**, D490-498, doi:10.1093/nar/gks1211. 595 42 Taufik, I., Kedrov, A., Exterkate, M. & Driessen, A. J. 2013. Monitoring the 596 4145-4153, activity of single translocons. *J Mol Biol* **425**, 597 doi:10.1016/j.jmb.2013.08.012. 598 43 Van den Berg, B. et al. 2004. X-ray structure of a protein-conducting 599 channel. Nature 427, 36-44, doi:10.1038/nature02218. 600 van der Laan, M., Bechtluft, P., Kol, S., Nouwen, N. & Driessen, A. J. 2004. 44 601 F1F0 ATP synthase subunit c is a substrate of the novel YidC pathway for 602 membrane protein biogenesis. J Cell Biol 165. 213-222. 603 doi:10.1083/jcb.200402100. 604 Wagenknecht, T., Grassucci, R. & Frank, J. 1988. Electron microscopy and 45 605 computer image averaging of ice-embedded large ribosomal subunits 606 from Escherichia coli. J Mol Biol 199, 137-147. 607 46 Yu, Z., Koningstein, G., Pop, A. & Luirink, J. 2008. The conserved third 608 transmembrane segment of YidC contacts nascent Escherichia coli inner

609	membrane	proteins.	J	Biol	Chem	283,	34635-34642,
610	doi:10.1074/j	bc.M8043442	200.				
611							
612							
613							

614 **FIGURE LEGENDS**

615

616 Figure 1

617 Evolutionary covariation based structural model of E. coli YidC

618 **a:** Membrane topology of YidC, with helix colouring as in all subsequent Figures.

b: Matrix of coupling strengths between pairs of YidC residues based on an
alignment of 2366 non-redundant sequences. Helix-helix pairs with posterior

probabilities higher than 57% are outlined in boxes; the 50 residue-residue pairswith highest coupling coefficients are indicated with red crosses.

623 **c:** Overall arrangement of TM helices viewed from the cytoplasm based on the 624 prediction of helix-helix pairs (black lines) and exposure to lipid (yellow) or 625 protein (green). The first residue of each helix is indicated with an asterisk.

d: Linear representation of YidC with the seven most probable helix-helix pairs

627 indicated by arches, with thicknesses approximating posterior probabilities.

628 e & f: Side view and cytoplasmic view, respectively, of the *E. coli* YidC model

based on covariation analysis, with predicted residue-residue pairs indicated byyellow pseudobonds.

631

632 Figure 1-figure supplement 1:

633 a: Calibration plots for the prediction of helix-helix interactions.

Calibration plots for dataset #2 (left), dataset #3 (middle) and combined
datasets #2 and #3 (right). The empirical fraction of true positives is plotted
depending on the uncalibrated probability (raw score) obtained from our
method. Points correspond to empirical averages over bins of 60 predictions
(ordered by increasing uncalibrated probability). Lines correspond to maximum
likelihood fits of the calibration plots using a transformed Bernoulli distribution
with 4 parameters.

641 **b:** Histogram of posterior probabilities for helix-helix interactions.

Distribution of predicted calibrated posterior probabilities for YidC (TM2 – TM6)
which contains 7 predicted helices, thus 21 possible helix-helix contacts. The
histogram of predicted probabilities shows the specificity of the predictions:
there is a large gap between 15% and 55% probability and most possible
contacts have probability < 15%.

647 Figure2:

648 **Covariation-based model** *vs* **homology model**

649 Comparison of the *E. coli* YidC covariation-based model (a & b) to a homology
650 model of *E. coli* YidC based on the crystal structure of BhYidC2 (3WO6) (c & d).
651 Predicted residue-residue pairs are indicated by yellow pseudobonds. Note that
652 extracellular helix 1 (white) was not present in our multiple sequence alignment
653 and is thus not included in the model.

- 654
- 655 Figure 2-figure supplement 1:

656 Local deviations among YidC structures

a: Smoothed Cα distances between the two BhYidC2 crystal forms (3W06 *vs*3W07, red), between our model of *E. coli* YidC and 3W06 (green) and between
our model and 3W07 (blue). b: Overall root mean square deviations (RMSD)
between (the TM helices of) our model of *E. coli* YidC and the two BhYidC2
crystal forms.

- 662
- 663 Figure 2-figure supplement 2:

Top 50 scoring residue-residue pairs in covariation analysis

Table showing the 50 residue-residue pairs with the highest covariation scores, and the distances between the C β atoms in the final model of the 39 pairs that were used as constraints for model building. For comparison, the corresponding distances in 3WO6 are also given. The eleven residue-residue pairs that were excluded for model building are in italics, with the reason for their exclusion indicated on the right.

671

672 Video 1:

673 Conformational states of YidC

Animation showing conformational differences in YidC starting from BhYidC2 crystal form 1 (3W06), towards crystal form 2 (3W07) and ending with our covariation based YidC model. Views are from within the membrane (left) and from the cytoplasm (right). Note the movement of the HPD and the closing of the hydrophilic groove between TM3 (orange) and TM5 (green).

680 Figure 3:

681 Molecular dynamics simulation of the YidC model

682 **a:** Side view (left) and cytoplasmic view (right) of the stable YidC model after a

683 500 ns MD simulation in a lipid bilayer composed of 3:1 POPE:POPG.

- 684 **b**: Ribbon representation of the stable model according to inter-helix energy (in
- 685 kcal/mol), blue: -7.5 to -1; white: -1 to -0.002; red: \geq -0.00.2. Residues that 686 inactivate YidC upon mutagenesis are indicated by spheres.
- 687 **c**: Ribbon representation of the stable model according to flexibility (in $Å^2$), blue: 688 0.04 to 0.09; white: 0.09-1; red: ≥1.0.
- 689 d: In vivo complementation assay of YidC mutants T362A (TM2) and Y517A 690 (TM6).
- 691 e: Thickness of the cytoplasmic and periplasmic leaflet of the simulated bilayer 692 after 500 ns, highlighting the membrane thinning effect in the vicinity of YidC. 693 The membrane surface is defined by positions of polar head groups in the lipids, 694 and thickness at a given point on the surface is taken to be the shortest distance 695 between the head groups from opposite leaflets. The thickness values are 696 averaged over the MD trajectory and presented as a contour plot on the 697 membrane surface with a color-scale from red, indicating thicker region 698 representing bulk bilayer lipids, to blue showing thinned regions close to YidC 699 suggesting hydrophobic mismatch.
- 700 **f**: Distribution of hydrophobic (red) and hydrophilic residues (blue) in YidC at 701 various heights of the membrane, highlighting the hydrophilic environment in 702 the center of YidC on the cytoplasmic side.
- 703

704 Figure 3-figure supplement 1:

705 **Complementation of MD-based mutants**

706 In vivo complementation assay of YidC mutants identified as structurally 707 important by MD simulations. Positions in YidC that were also identified by 708

covariation analyses are indicated in the right column.

- 709
- 710 Figure 3-figure supplement 2:
- 711 **Expression of MD-based mutants**

Western blot of whole FTL10 cells grown on arabinose or glucose, showing the
stable expression of inactive YidC mutants that were identifed by MD
simulations.

715

716 Figure 4:

717 Cryo-EM structure of RNC bound YidC and structural model of the active718 state

a: Side view of the ~8 Å resolution cryo-EM based electron density of the
RNC:YidC complex, with the small subunit depicted in yellow, the large subunit
in grey, P-site tRNA and nascent chain in green, YidC in red and the detergent
micelle in blue.

723 **b:** As in **a**, but sliced through the ribosomal exit tunnel.

724 c: Validation of the active state model by disulphide crosslinking. RNCs carrying 725 the mutant $F_0c^{(G23C)}$ were reconstituted with the indicated single cysteine YidC 726 mutants, oxidized, applied to a linear sucrose gradient and harvested from the 727 70S peak before SDS-PAGE and western blotting. Immunodetection was 728 performed with antibodies raised against the HA-tag (located in the nascent 729 chain inside the ribosomal exit tunnel) and anti-YidC antibodies. YidC, nascent 730 chain-tRNA (NC-tRNA) and the expected crosslink product (NC-tRNA x YidC) are 731 indicated.

d-f: Structural model of YidC during membrane protein insertion, viewed from
two sides within the membrane (d & e) and from the cytoplasm (f). The
detergent micelle was removed for clarity, the TM helix of F₀c is depicted in
magenta, and the disulphide crosslink between YidC and F₀c with -SS-.

736

Figure 4-figure supplement 1:

738 **Comparison of the active states of YidC and SecY**

Left: Molecular model of YidC during co-translational translocation of F₀c, and
the contour of active SecY. Middle: Composite model of active YidC with F₀c
replaced by the hydrophilic part of nascent FtsQ as found in active SecY. Right:
Molecular model of SecY during co-translational translocation of FtsQ. For
clarity, the N-terminal signal anchor of FtsQ was omitted.

Figure 4-figure supplement 2:

746 Negative control for RNC-YidC crosslinking

747 Crosslinking was performed with a cysteine-less F_0c RNC as described in the

748 legend to Figure 3c. A poorly reproducible unknown product is indicated with an749 asterisk.

- 750
- 751 Figure 5:

752 **Contacts between active YidC and the ribosome**

a & b: Close-up views from within the membrane region highlighting the contact
between H59 of the ribosome and the 2/3 loop of YidC (a) and ribosomal protein
uL23 and the 4/5 loop of YidC (b). Residues that inactivate YidC upon
mutagenesis or deletion are indicated by magenta spheres.

c: *In vivo* complementation assay of YidC point mutants D488A, D488K, deletion

- mutant Δ 487-489 and the double mutants Y370A/Y377A and Y370F/Y377F.
- **d:** Periplasmic view of the active ribosome-bound YidC model, with the YidC
- contour outlined in red. The polypeptide exit tunnel is indicated with an asterisk.
- 761 e: Cartoon based comparison of active SecY (left) and active YidC (right) during
- 762 membrane insertion of FtsQ and F₀c, respectively. The ribosome is depicted in
- 763 grey, the aqueous channel in SecY as well as the hydrophilic environment within
- YidC are shaded blue, hydrophobic TM domains of the substrates are depicted
- magenta, hydrophilic parts in green and the P1 domain by a dashed oval.

766

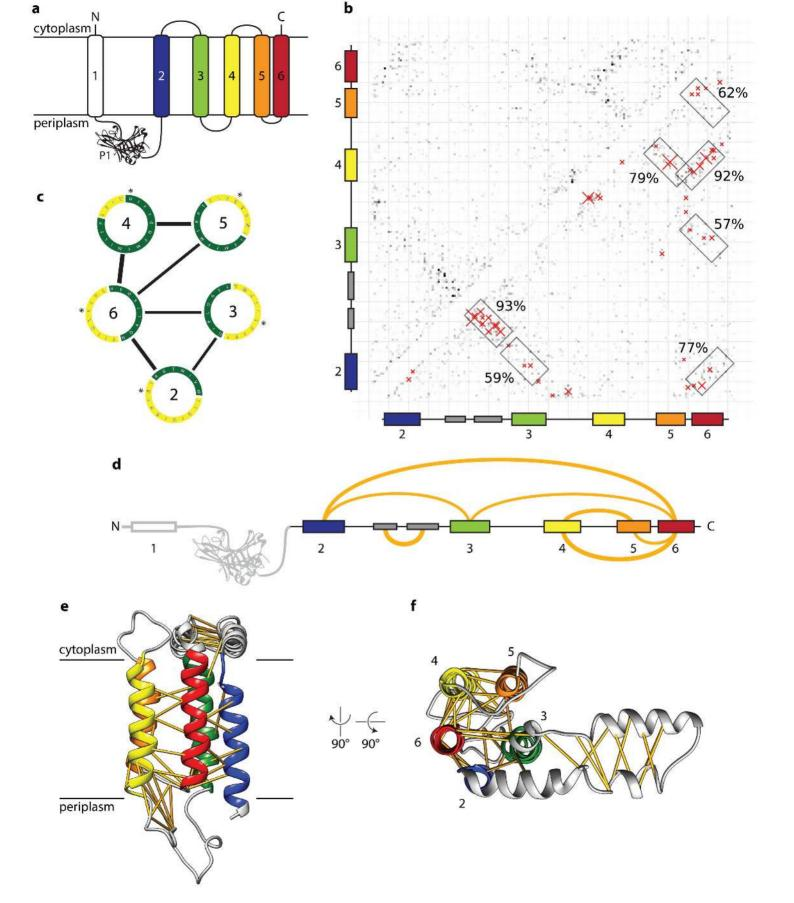
Figure 5-figure suppement 1:

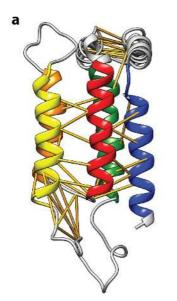
768 **Complementation of ribosome interaction mutants**

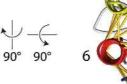
- 769 *In vivo* complementation assay of YidC mutants involved in ribosome binding.
- 770
- Figure 5-figure supplement 2:

772 **Expression of ribosome interaction mutants**

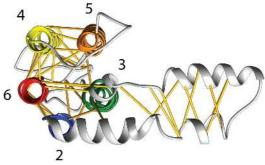
- 773 Western blot of whole FTL10 cells grown on arabinose or glucose, showing the
- stable expression of inactive YidC mutants that interact with the ribosome.

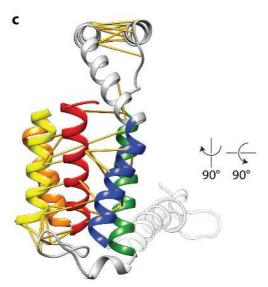


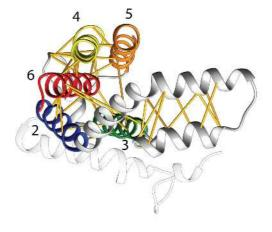




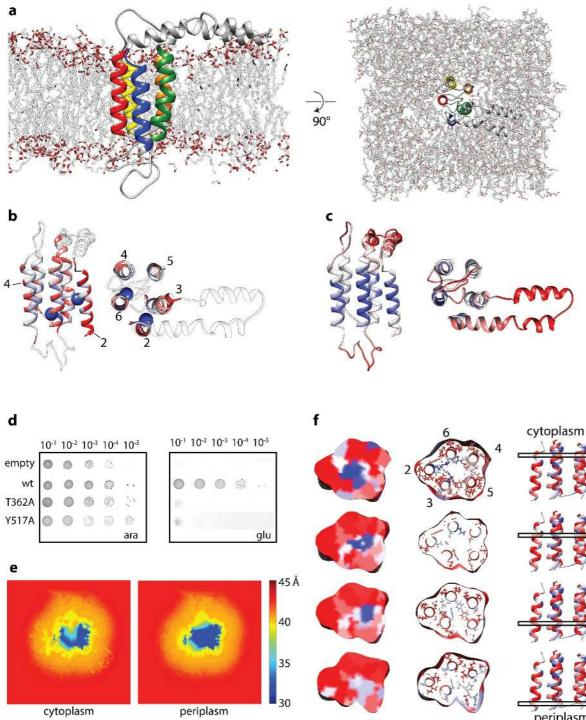
d



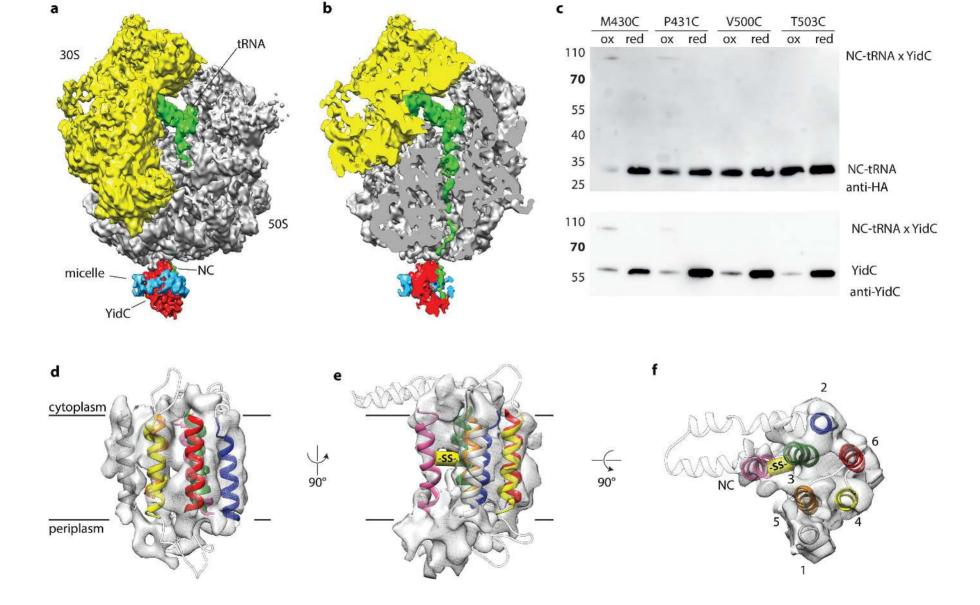


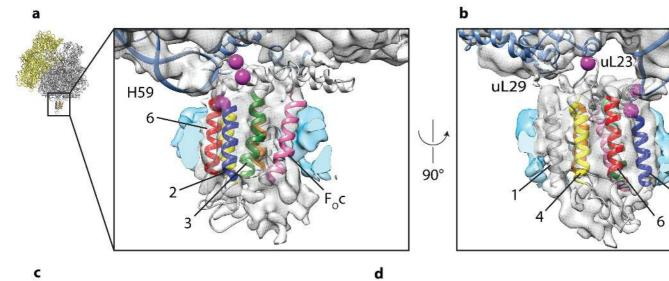


b

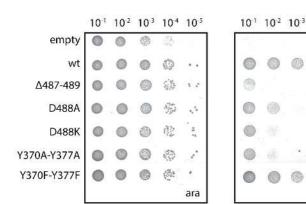


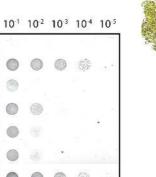
periplasm



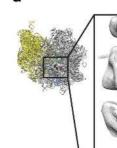


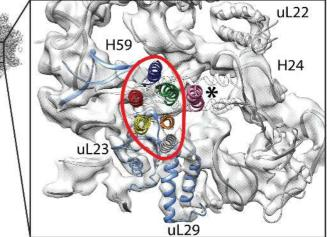
d





glu





H59

